Molecular diffusion and slip boundary conditions at smooth surfaces with periodic and random nanoscale textures

Nikolai V. Priezjev
Department of Mechanical Engineering, Michigan State University, East Lansing, Michigan 48824, USA

The influence of periodic and random surface textures on the flow structure and effective slip length in Newtonian fluids is investigated by molecular dynamics (MD) simulations. We consider a situation where the typical pattern size is smaller than the channel height and the local boundary conditions at wetting and nonwetting regions are characterized by finite slip lengths. In the case of anisotropic patterns, transverse flow profiles are reported for flows over alternating stripes of different wettability when the shear flow direction is misaligned with respect to the stripe orientation. The angular dependence of the effective slip length obtained from MD simulations is in good agreement with hydrodynamic predictions provided that the stripe width is larger than several molecular diameters. We found that the longitudinal component of the slip velocity along the shear flow direction is proportional to the interfacial diffusion coefficient of fluid monomers in that direction at equilibrium. In case of random textures, the effective slip length and the diffusion coefficient of fluid monomers in the first layer near the heterogeneous surface depend sensitively on the total area of wetting regions. © *2011 American Institute of Physics*. [doi:10.1063/1.3663384]

I. INTRODUCTION

Modeling fluid flows over chemically or topographically patterned substrates is important for micro- and nanofluidic applications involving mixing[1] and separation processes.[2] As the surface to volume ratio increases, the role of hydrodynamic boundary conditions in determining fluid velocity profiles becomes dominant. It is well recognized now that the classical no-slip boundary condition can, in principle, be violated and the velocity profiles can be significantly affected by the interfacial slip.[3] The degree of slip is usually quantified in terms of the Navier slip length, which is defined as a distance between the real interface and imaginary plane where the extrapolated tangential velocity component vanishes. The magnitude of the slip length for smooth nonwetting surfaces is typically on the order of tens of nanometers;[4–8] however, in special cases of nanoengineered superhydrophobic surfaces, slip lengths in the micrometer range were reported.[9–12] Although the Navier-Stokes equation with slip boundary conditions is often used to model small scale flows, the limits of validity of the continuum description of complex flows at nanometer scales remain not fully understood.[3]

In recent years, a number of molecular dynamics (MD) studies have examined factors that determine the magnitude of the slip length at interfaces between crystalline surfaces and monatomic liquids.[13–28] One of the most important conclusions is that the degree of slip strongly correlates with the in-plane structure in the first fluid layer induced by the periodic surface potential.[15] An estimate of the low-shear-rate limit of the slip length can be obtained via the Green-Kubo relation between the friction coefficient at the interface and the time integral of the autocorrelation function of the lateral force that acts on the adjacent fluid from the solid wall.[18] In general, when the surface energy is weak, the slip length is constant only at relatively low shear rates and it increases nonlinearly at high shear rates.[16] It was recently demonstrated that the linear regime of slip holds when the slip velocity of the first fluid layer is smaller than the diffusion rate of fluid monomers over the distance between the nearest minima of the periodic surface potential at equilibrium.[29] It was also found that at sufficiently high shear rates, the slip length becomes anisotropic for dense walls with weak surface energy; and, in particular, the slip length increases when the flow is oriented along the crystallographic axis of the wall lattice.[29]

Several studies considered the flow of a Newtonian fluid over surfaces patterned with stripes of different wettability using both molecular dynamics and continuum simulations.[30–33] In the presence of flow, a heterogeneous surface with mixed boundary conditions induces spatial variations in the velocity profiles. The flow profiles averaged on length scales larger than the typical pattern size can be used to define the *effective slip length*, which describes the flow away from the surface. The comparative analysis between MD and continuum simulations demonstrated that there is an excellent agreement between the velocity profiles and effective slip lengths for stripe widths larger than approximately 30 molecular diameters for flow configurations either parallel or perpendicular to the stripe orientation.[31] Later studies have shown that similar conclusions hold for slip flows of Newtonian[34,35] and polymeric[36] fluids over periodically corrugated surfaces. In a more general situation, when the mean flow direction is not aligned with the symmetry axis of surface patterns, it is expected that the slip velocity will acquire a non-zero transverse component. In MD simulations, the transverse velocity profiles were reported in force-driven flows over flat surfaces with asymmetric distribution of wetting regions[33] and in spiral flows inside a cylindrical channel.[37] One of the goals of the present study is to perform a detailed comparative

analysis of the effective slip length and velocity fields in flows around anisotropic textured surfaces using MD simulations and recent analytical results.[38–40]

The Navier slip boundary condition for flows over arbitrary patterned surfaces can be formulated in tensor form, i.e., the apparent slip velocity vector is equal to the product of normal traction and an interfacial mobility tensor.[41–43] It was suggested that at the microscopic level, the mobility tensor is related to the interfacial diffusivity per unit area.[41] Recently, it was also proven that for steady noninertial flows over surfaces perturbed by arbitrary periodic height and local slip fluctuations, the mobility tensor is always symmetric.[44] Using the theory of transport in heterogeneous media, rigorous bounds on the effective slip length were obtained for arbitrary two-component texture with given area fractions and local slip lengths.[45,46] In particular, it was shown that parallel (perpendicular) stripe orientation with respect to the mean flow direction results in maximum (minimum) slip flow in a thin channel.[45] In case when the mean flow is not parallel or perpendicular to stripes, the angular dependence of the effective slip length was derived analytically[38,41] and later verified by lattice Boltzmann simulations.[47] One of the motivations of the current study is to examine the microscopic justification of the tensor formulation of the Navier slip condition for surfaces with anisotropic textures.

In this paper, the velocity fields and diffusion of fluid molecules near interfaces between simple fluids and surfaces patterned with anisotropic and random textures are studied by molecular dynamics simulations. For flows around parallel stripes of different wettability, the transverse and longitudinal velocity components and the effective slip length are compared against hydrodynamic predictions. We will show that the directional diffusion coefficient for fluid molecules in contact with wall atoms correlates well with the effective slip length as a function of the flow direction with respect to the stripe orientation. In case of random wetting patterns, the effective slip length depends sensitively on the total area of wetting regions, in agreement with simple physical arguments.

The rest of the paper is organized as follows. The details of molecular dynamics simulations, parameter values, and thermostatting procedure are described in Sec. II. The results for the effective slip length at surfaces with periodic and random textures and the numerical analysis of the interfacial diffusion of fluid molecules are presented in Sec. III. The conclusions are given in Sec. IV.

II. DETAILS OF MOLECULAR DYNAMICS SIMULATION MODEL

The schematic setup of the channel geometry and the orientation of wetting and nonwetting regions of the stationary lower wall are illustrated in Figure 1. The steady shear flow is induced by the upper wall moving with a constant velocity in the xy plane. The structure of three-dimensional flow fields in the confined fluid is determined by the local boundary conditions at the patterned lower wall and the orientation of the upper wall velocity with respect to the stripe direction.
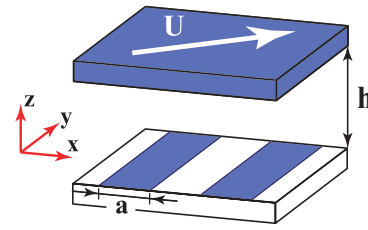

FIG. 1. A schematic representation of the channel geometry and surface patterns indicated by the blue color (wetting regions) and white color (nonwetting regions). Steady shear flow is induced by the upper wall moving with a constant velocity U in the xy plane at an angle θ with respect to the $\hat{x}$ direction. The lower patterned wall is stationary.

The pair interaction between fluid monomers ($N_f = 6000$) is modeled via the truncated Lennard-Jones (LJ) potential

$$V_{LJ}(r) = 4\varepsilon \left[\left(\frac{\sigma}{r} \right)^{12} - \left(\frac{\sigma}{r} \right)^{6} \right], \quad (1)$$

where ε and σ are the energy and length scales of the fluid phase, and the cutoff radius is $r_c = 2.5\sigma$. Wall atoms interact with fluid monomers through a modified LJ potential with adjustable strength of the attractive term

$$\widetilde{V}_{LJ}(r) = 4\varepsilon \left[\left(\frac{\sigma}{r} \right)^{12} - \delta \left(\frac{\sigma}{r} \right)^{6} \right], \quad (2)$$

where the parameter $\delta = 1.0$ for wetting regions and $\delta = 0.1$ for nonwetting regions and the rest of the parameters are the same, i.e., $\varepsilon_{wf} = \varepsilon$, $\sigma_{wf} = \sigma$, and $r_c = 2.5\sigma$. The wall atoms do not interact with each other. For the results presented in Sec. III, the parameter $\delta = 1.0$ was fixed for the upper wall atoms, while the lower wall is either homogeneous ($\delta = 1.0$ or $\delta = 0.1$) or patterned with periodic stripes or random wetting regions.

The solid walls are constructed of two layers of the face-centered cubic (fcc) lattice with density $\rho_w = 2.3\sigma^{-3}$. Each layer is composed of 576 lattice sites arranged on the (111) plane with [11$\bar{2}$] orientation parallel to the $\hat{x}$ direction. The nearest-neighbor distance between lattice sites within the (111) plane is 0.85σ. The wall atoms are attached to the lattice sites by harmonic springs. The system dimensions in the xy plane (parallel to the confining walls) were kept fixed $L_x = 17.67\sigma$ and $L_y = 20.41\sigma$, and the distance between wall lattice planes in contact with fluid molecules was set $h = 21.54\sigma$. The fluid density is defined as a ratio of the total number of fluid monomers to the volume accessible to the fluid phase $\rho = N_f/L_x L_y (h - \sigma) = 0.81\sigma^{-3}$. Periodic boundary conditions for fluid monomers and wall atoms were imposed along the $\hat{x}$ and $\hat{y}$ directions. The motion of the upper wall with a constant velocity oriented at an angle θ with respect to the $\hat{x}$ axis was modelled by translating the fcc lattice sites and applying periodic boundary conditions in the xy plane at each time step. Figure 2 shows a snapshot of the fluid phase confined between atomically smooth walls. In this particular case, the upper wall velocity is oriented perpendicular to the stripe direction.

The motion of wall atoms was coupled to an external heat bath by adding Langevin noise and friction terms to all three components of the equations of motion, e.g., in the $\hat{x}$ direction
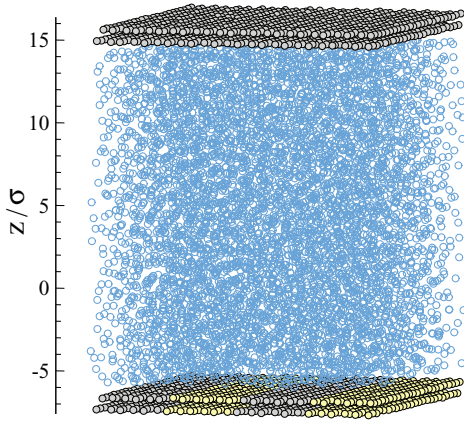
FIG. 2. A snapshot of 6000 fluid monomers (open blue circles) confined between atomistic walls patterned with wetting (filled gray circles) and nonwetting (filled yellow circles) regions. The width of stripes at the lower stationary wall is $a = 4.42\sigma$ and the upper wall velocity is $U = 0.1\sigma/\tau$.

the equation is given by

$$m_w \ddot{x}_i + m_w \Gamma \dot{x}_i = -\sum_{i \neq j} \frac{\partial \widetilde{V}_{\mathrm{LJ}\, ij}}{\partial x_i} - \frac{\partial V_{sp}}{\partial x_i} + f_i, \quad (3)$$

where the mass of a wall atom is $m_w = 100\, m$, the friction coefficient is $\Gamma = 2.0\tau^{-1}$, and f_i is a random force with zero mean and variance $\langle f_i(0) f_j(t)\rangle = 2mk_B T\Gamma \delta(t)\delta_{ij}$ determined from the fluctuation-dissipation theorem. The temperature of the Langevin thermostat is $T = 1.1\, \varepsilon/k_B$, where k_B is the Boltzmann constant. The wall atoms were tethered to the fcc lattice sites under the harmonic potential $V_{sp} = \frac{1}{2}\kappa\, r^2$ with the spring stiffness coefficient $\kappa = 2000\varepsilon/\sigma^2$. It was previously shown that a sufficiently large value of the stiffness coefficient does not affect the slip length at the interface between monatomic fluids and dense crystalline walls.[23] The equations of motion for wall atoms and fluid monomers were solved using the fifth-order Gear predictor-corrector scheme[48] with a time step $\triangle t = 0.005\tau$, where $\tau = \sqrt{m\sigma^2/\varepsilon}$ is the LJ time scale. Thus, the oscillation time $2\pi\sqrt{m_w/\kappa} \approx 1.4\tau$ of wall atoms is much larger than the integration time step. Typical values for liquid argon are $\sigma = 0.34\,\mathrm{nm}$, $\varepsilon/k_B = 120\,\mathrm{K}$, and $\tau = 2.16 \times 10^{-12}\,\mathrm{s}$.[48]

A common practice in non-equilibrium MD simulations is to apply the Langevin thermostat only in the direction of motion perpendicular to the plane of shear in order to maintain constant temperature of the fluid phase.[15, 16] It is expected, however, that if the orientation of the upper wall velocity is restricted to $0° < \theta < 90°$ in the system shown in Fig. 1, then the fluid flow near the lower patterned wall will have non-zero components of the averaged velocity fields in all spatial dimensions, and, therefore, the Langevin friction term applied to fluid monomers might bias the flow profile. To test the dependence of our results on the thermostatting procedure, we performed simulations with $a = 8.84\,\sigma$ and the upper wall velocity $U = 0.1\sigma/\tau$ oriented at $\theta = 45°$ relative to the $\hat{x}$ direction for two cases where the Langevin thermostat with $\Gamma = 1.0\tau^{-1}$ was applied to the equations of motion for fluid monomers in the direction either perpendicular to the plane of shear or parallel to the $\hat{z}$ direction. After

averaging over thermal fluctuations, we observed a slight difference in the velocity profiles near the lower wall which resulted in a discrepancy between slip lengths of about $0.5\,\sigma$. To eliminate the uncertainty associated with the friction term, in the present study, the Langevin thermostat was applied only to the equations of motion for wall atoms. The viscous heat in the fluid phase was efficiently removed via interaction of fluid monomers with thermal wall atoms so that the fluid temperature remained constant $T_f = (1.10 \pm 0.01)\varepsilon/k_B$, even at the highest upper wall velocity $U = 0.1\sigma/\tau$. A similar thermostatting procedure in sheared fluids confined by thermal walls was implemented in previous MD studies.[27, 49, 50]

In the present study, the simulations were performed at relatively low shear rates $\dot\gamma \lesssim 0.005\tau^{-1}$, which required averaging of the velocity profiles over long time intervals (up to $10^6\tau$) within horizontal bins of thickness $\Delta z = 0.01\sigma$. Likewise, the fluid density profiles were computed within narrow bins of thickness $\Delta z = 0.01\sigma$ to resolve fine details of the layered structure near interfaces. The structure factor was computed in the first fluid layer according to $S(\mathbf{k}) = |\sum_{j=1}^{N_\ell} e^{i\mathbf{k}\cdot\mathbf{r}_j}|^2/N_\ell$, where $\mathbf{k}$ is a two-dimensional wave vector, $\mathbf{r}_j = (x_j, y_j)$ is the position of the jth monomer, and N_ℓ is the total number of monomers within the layer.[15] The fluid viscosity $\mu = (2.15 \pm 0.15)\varepsilon\tau\sigma^{-3}$ was previously found to be rate independent for $\dot\gamma \lesssim 0.072\tau^{-1}$ and insensitive to the temperature variation in the range of $1.1 \leq Tk_B/\varepsilon \leq 1.35$.[34] An estimate of the maximum value of the Reynolds number based on $U = 0.1\,\sigma/\tau$ and no-slip boundary conditions is $Re = \rho h U/\mu \approx 0.77$, which is clearly indicative of laminar flow in the channel.

III. RESULTS

A. Fluid density and velocity profiles for homogeneous walls

We first consider steady shear flow in the channel with a homogeneous lower wall, which is either wetting ($\delta = 1.0$) or nonwetting ($\delta = 0.1$). It is well known that the presence of a flat crystalline surface promotes the formation of a layered structure in the adjacent fluid (e.g., see Ref. 51). An example of fluid density profiles is shown in Fig. 3(a). As is evident, the fluid layering is most pronounced near interfaces, the amplitude of density oscillations gradually decays on distances of about five molecular diameters away from the solid walls, and the fluid density is uniform in the middle of the channel.

The interaction between fluid monomers and wall atoms is controlled by the strength of the attractive term in the LJ potential. When the parameter δ in Eq. (2) is reduced, then the well depth of the potential function decreases and the pairwise separation, where the potential energy reaches a minimum value, increases. For comparison, the minimum of the full LJ potential with $\delta = 1.0$ in Eq. (2) occurs at $r = \sqrt[6]{2}\,\sigma \approx 1.12\sigma$ and equals $\widetilde{V}_{\mathrm{LJ}}(1.12\,\sigma) = -\varepsilon$, while the modified LJ potential with $\delta = 0.1$ has a much lower well depth $\widetilde{V}_{\mathrm{LJ}}(1.65\,\sigma) = -0.01\varepsilon$. Therefore, it is not surprising that the amplitude of the first fluid layer near the nonwetting lower wall in Fig. 3(a) is significantly reduced and its location is shifted away from the wall. Note also that, due to a pronounced fluid layering near the wetting lower wall, the
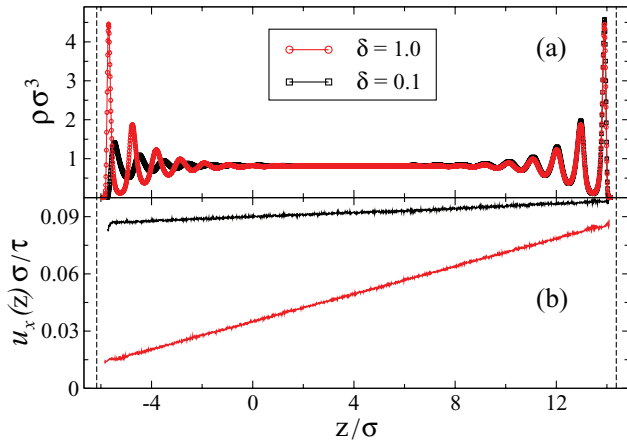
FIG. 3. Averaged (a) density and (b) velocity profiles across the channel for wetting $\delta = 1$ (red circles) and nonwetting $\delta = 0.1$ (black squares) lower walls. The upper wall velocity in the $\hat{x}$ direction is $U = 0.1\sigma/\tau$. The vertical axes at $z/\sigma = -6.67$ and 14.87 coincide with the location of the fcc lattice planes in contact with fluid molecules. The vertical dashed lines at $z/\sigma = -6.17$ and 14.37 indicate the location of liquid-solid interfaces.
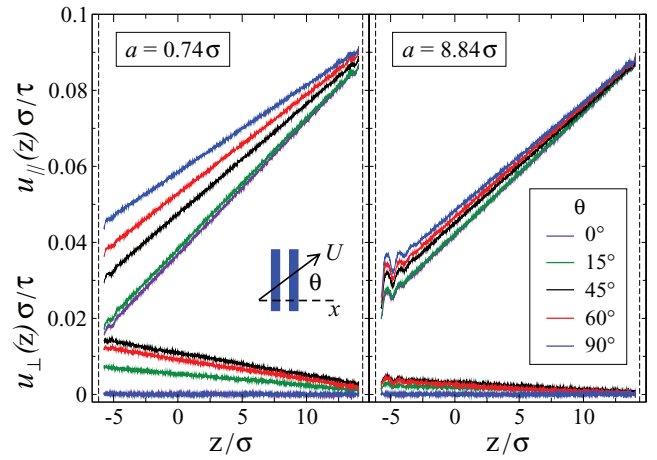

FIG. 4. Averaged longitudinal (upper set of curves) and transverse (lower set of curves) velocity profiles for the indicated values of θ and stripe widths $a = 0.74\sigma$ (left panel) and $a = 8.84\sigma$ (right panel). The vertical axes coincide with the location of the fcc lattice planes at $z/\sigma = -6.67$ and 14.87. The vertical dashed lines at $z/\sigma = -6.17$ and 14.37 indicate liquid-solid interfaces.

amplitude of density oscillations near the upper wall is slightly smaller in the wetting case. Finally, we have checked that the density profiles reported in Fig. 3(a) for the upper wall velocity $U = 0.1\sigma/\tau$ are the same as those computed in the absence of shear flow (not shown).

The averaged fluid velocity profiles for wetting and nonwetting lower walls are presented in Fig. 3(b). In both cases, the velocity profiles are linear across the channel; however, the slip velocity is much higher near the nonwetting lower wall. A slight downward curvature in the velocity profile near the nonwetting surface might be related to the fact that only fluid monomers with relatively large velocity component in the $\hat{z}$ direction can penetrate more deeply into the solid wall and, thus, the tangential velocity in that region is computed from biased velocity distribution. To compute the slip length, we define the location of liquid-solid interfaces (see vertical dashed lines in Fig. 3) at the distance 0.5σ away from the fcc wall lattice planes in contact with fluid monomers. For flows over homogeneous walls, the slip length is determined from the linear fit to the velocity profiles excluding regions of about 2σ near interfaces. Depending on the wall-fluid interaction, the slip lengths are $b_w = (3.6 \pm 0.8)\sigma$ for wetting surfaces and $b_n = (156 \pm 10)\sigma$ for nonwetting surfaces. Within the reported error bars, the slip lengths are independent of the shear flow orientation relative to the fcc wall lattice. It was shown that at low shear rates, $\dot{\gamma} \lesssim 0.005\tau^{-1}$, considered in the present study, the slip length at an interface between smooth crystalline walls and monatomic fluids is rate independent.[16]

B. Anisotropic slip lengths for periodically patterned walls

We next study the effects of shear flow orientation and stripe width on the flow structure in the channel with the lower stationary wall patterned with alternating stripes of different wettability, as shown in Fig. 1. In this geometry, the tex-

tured lower wall induces wavy perturbations in simple shear flow which penetrate into the fluid domain on a length scale of about a stripe width, and the slip velocity at the lower wall is not parallel to the upper wall velocity when $0° < \theta < 90°$. In this section, we only consider alternating stripes of equal width, which are measured $a = L_x/n$, where integer $n = 2, 4, 8, 12,$ and 24. Thus, in all cases examined, the stripe width ($a/\sigma = 8.84, 4.42, 2.21, 1.47, 0.74$) is smaller than the channel height $h = 21.54\sigma$; and, therefore, the longitudinal velocity profiles are expected to be linear across the channel except in the region of about a near the lower wall. In what follows, we denote the longitudinal component of the fluid velocity profile (parallel to the upper wall velocity) by $u_\parallel(z)$ and the transverse component of the velocity profile by $u_\perp(z)$, which is perpendicular to the direction of U.

The problem of anisotropic slip flow over an array of periodic stripes of mixed wettability was addressed analytically assuming that the stripe width is much smaller than the fluid domain.[38–41] In particular, it was shown that the angular dependence of the effective slip length is given by

$$L_s(\theta) = b_\perp \cos^2\theta + b_\parallel \sin^2\theta, \qquad (4)$$

where $b_\perp$ and $b_\parallel$ are, respectively, slip lengths for flows perpendicular ($\theta = 0°$) and parallel ($\theta = 90°$) to the stripe orientation.[38,40] If the local slip lengths at wetting and nonwetting regions are finite and independent of the flow direction, then $b_\parallel > b_\perp$ and in the special case of stick-perfect slip stripes $b_\parallel = 2\,b_\perp$.[40,52] From the solution of the Stokes equation with mixed boundary conditions,[39,40] the ratio of slip velocities in longitudinal and transverse directions can be calculated as a function of the flow orientation

$$\frac{u_\perp^s}{u_\parallel^s} = \frac{(b_\parallel - b_\perp)\sin\theta\,\cos\theta}{b_\perp\cos^2\theta + b_\parallel\sin^2\theta}. \qquad (5)$$

In the limiting cases when the flow direction is perpendicular or parallel to the stripe orientation or when the surface is homogeneous (i.e., $b_\parallel = b_\perp$), the transverse slip velocity in Eq. (5) vanishes. As an aside, the continuum analysis also
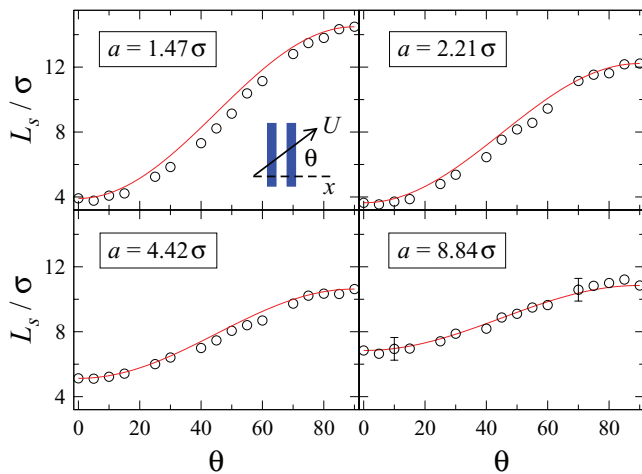
FIG. 5. Variation of the effective slip length L_s/σ as a function of θ for the indicated values of the stripe width. The MD data are shown by open circles. The red curves are hydrodynamic predictions computed using Eq. (4).

FIG. 6. The ratio of transverse and longitudinal components of the slip velocity as a function of θ. The MD data are shown by open circles. The solid red curves are continuum predictions calculated using Eq. (5). The dashed blue curve is Eq. (5) where $b_{\perp, ||}$ are defined with respect to the location of the first fluid layer (see text for details).

predicts that the transverse velocity component is maximum when $\theta = 45°$.[39]

Examples of longitudinal and transverse velocity profiles for the smallest ($a = 0.74\sigma$) and largest ($a = 8.84\sigma$) stripe widths are presented in Fig. 4 for selected values of θ. In both cases, the longitudinal velocity component is maximum (minimum) when the upper wall velocity is parallel (perpendicular) to the stripe orientation, and the transverse flow is maximum when $\theta = 45°$, in agreement with the continuum analysis.[39,40] If the stripe width is about the molecular size, the alternating surface potential [$\delta = 1.0$ and 0.1 in Eq. (2)] represents an effectively roughened surface for the flow component perpendicular to the stripe orientation. As a consequence, the location of the first fluid layer varies periodically above wetting and nonwetting regions [e.g., see Fig. 3(a)], and the slip velocity along the $\hat{x}$ direction (perpendicular to stripes) is reduced. In contrast, when the flow is parallel to stripes, fluid monomers are transported along homogeneous wetting or nonwetting regions, and the effect of surface roughness is absent. This explains the relatively large variation of the longitudinal slip velocity as a function of the flow orientation for the stripe width $a = 0.74\sigma$. For the largest stripe width $a = 8.84\sigma$, the velocity profiles acquire pronounced oscillations near the lower wall because of the mismatch between the location of peaks in density profiles above wetting and nonwetting regions [shown in Fig. 3(a)]. Similar effects were reported in the previous study where only flows parallel and perpendicular to stripes were considered.[31] For the results presented below, the effective slip length was computed by extrapolating the linear part of the longitudinal velocity profiles to zero velocity.

The angular dependence of the effective slip length for the indicated values of the stripe width is presented in Fig. 5. As expected, L_s monotonically increases as θ approaches $90°$. For a given stripe width, the values $b_{\perp}$ and $b_{||}$ were determined from the longitudinal velocity profiles and then used in Eq. (4) to compare the results of MD simulations with continuum predictions (shown by red curves in Fig. 5). The agreement between the MD data and continuum solution Eq. (4)
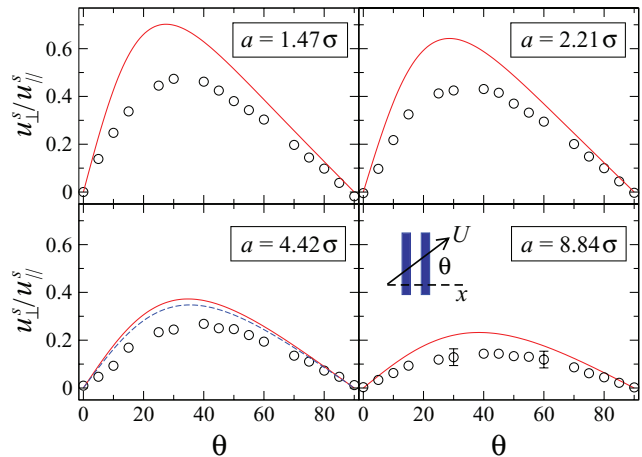
becomes progressively better as the stripe width increases up to $a = 8.84\sigma$. It should be mentioned that these results do not contradict the conclusion drawn from the previous study,[31] which demonstrated that the agreement between continuum analysis and MD simulations holds when the stripe width is larger than about 30 molecular diameters. In the context of the present study, this conclusion could be verified by computing $L_s(\theta)$ directly from the solution of the Stokes equation for the flow geometry shown in Fig. 1 with the local slip lengths at wetting and nonwetting regions extracted from MD simulations. Such an analysis was not performed in the current study.

As discussed above, the transverse flow appears when the upper wall velocity is neither parallel nor perpendicular to the stripe orientation. Next, we present a more detailed comparative analysis of the transverse slip velocity at the lower wall based on the MD data and the continuum solution Eq. (5). In MD simulations, the longitudinal and transverse slip velocity components of the first fluid layer were computed as follows:

$$u^s_{\perp, ||} = \int_{z_0}^{z_1} u_{\perp, ||}(z)\, \rho(z)\, dz \Big/ \int_{z_0}^{z_1} \rho(z)\, dz, \qquad (6)$$

where the limits of integration ($z_0 = -5.1\sigma$ and $z_1 = -5.8\sigma$) are defined by the width of the first peak in the density profile above the patterned lower wall. The ratio $u^s_{\perp}/u^s_{||}$ as a function of θ is plotted in Fig. 6. The results show that although the magnitude of the transverse slip velocity is largest when $\theta = 45°$, the maximum angle between the upper wall velocity and the slip velocity occurs when $\theta < 45°$. For example, this angle is about $25°$ for the stripe width $a = 1.47\sigma$ when $\theta = 30°$. Further, the MD values $b_{\perp}(a)$ and $b_{||}(a)$ were used in Eq. (5) to compute the ratio $u^s_{\perp}/u^s_{||}$ as a function of θ (see red curves in Fig. 6). The continuum solution Eq. (5) is only in qualitative agreement with the MD data. The discrepancy might be attributed to the roughness effect discussed earlier and to the fact that the stripe width is comparable to the fluid molecular size. Another possible contributing factor is the uncertainty in defining the exact location of the liquid-solid
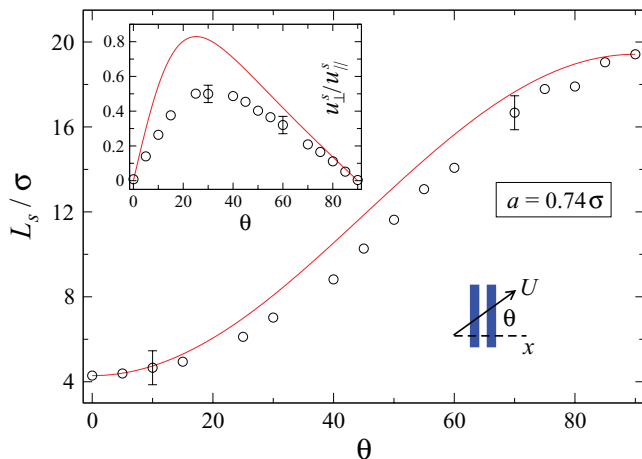
FIG. 7. The effective slip length L_s/σ as a function of θ for the stripe width $a = 0.74\sigma$. The continuum prediction, Eq. (4), is shown by the red curve. The inset shows the angular dependence of the ratio of slip velocities in transverse and longitudinal directions. The red curve in the inset is the prediction of Eq. (5).

FIG. 8. The mean square displacement of fluid monomers in the first layer near the lower patterned wall with the stripe width $a = 2.21\sigma$, when both walls are at rest. Each curve is computed by taking the component of the displacement vector along a line oriented at angles $\theta = 0°$, $25°$, $45°$, $60°$, $90°$ with respect to the $\hat{x}$ axis (from bottom to top). The dashed line with unit slope is plotted for reference. The lower inset shows an expanded view of the same data at large t. The upper inset shows a correlation between the in-plane diffusion coefficient and the effective slip length for the same set of θ. The straight blue line is the best fit to the data.

interface used for computing the effective slip length (e.g., see the vertical dashed lines in Fig. 4). Remember that the position of the first fluid layer is displaced by about σ from the fcc lattice plane. Thus, if the location of the interface is taken at the position of the first fluid layer, then the effective slip lengths become $b_{\perp,\|} \rightarrow b_{\perp,\|} + 0.5\sigma$. The corresponding continuum solution Eq. (5) is shown by the blue dashed curve in Fig. 6 when the stripe width is $a = 4.42\sigma$. Notice the small difference between continuum solutions, which, in general, is expected to be negligible when $b_{\perp,\|} \gg 0.5\sigma$. For completeness, the results for the smallest stripe width $a = 0.74\sigma$ are reported in Fig. 7. In this case, the discrepancy between the MD data and continuum solutions Eqs. (4) and (5) is most pronounced.

C. Interfacial diffusion near surfaces of patterned wettability

A tensorial generalization of the Navier slip condition for flows over anisotropic surfaces involves a relation between the normal traction at the interface and fluid slip velocity via an interfacial mobility tensor.[41] In analogy with the theory of Brownian motion, it was conjectured that the mobility of fluid molecules near anisotropic surfaces is directly related to the interfacial diffusivity per unit area.[41] Simply put, it implies that the effective slip length at the interface between a Newtonian fluid and a textured surface is proportional to the diffusion coefficient of fluid molecules near the surface. In the present study, the diffusion coefficient was estimated from two-dimensional trajectories of fluid monomers within the first layer near the patterned wall at equilibrium (i.e., when both walls are at rest).

The numerical analysis of the molecular displacement was performed only for those fluid monomers that remained in contact with the lower wall atoms (in the first fluid layer) during the diffusion time interval. It should be noted that it is important not to include fluid monomers further away from the patte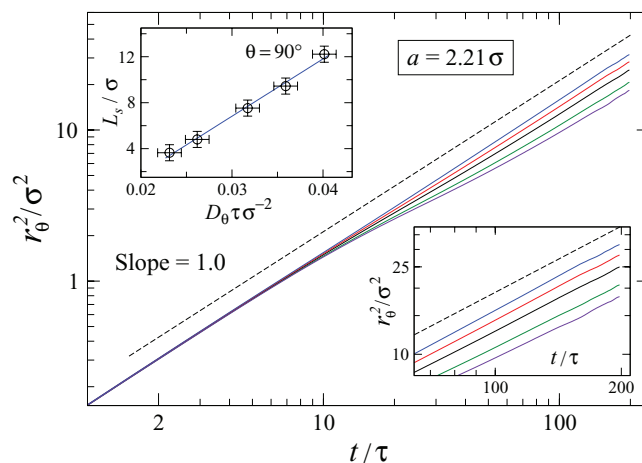rned wall because their diffusion in the xy plane quickly becomes isotropic. For example, it was recently shown that when the LJ fluid is confined in narrow slit-pores (with the channel height of about 5σ) and both walls are patterned with stripes of different wettability, then the mean square displacement (MSD) curves, which were averaged over all fluid molecules in the direction either parallel or perpendicular to stripes, nearly coincide with each other.[53]

Figure 8 shows the time dependence of the mean square displacement of fluid monomers near the lower wall with stripes of width $a = 2.21\sigma$. For each curve plotted in Fig. 8, the displacement vector in the xy plane was projected onto a line oriented at angles $\theta = 0°$, $25°$, $45°$, $60°$, $90°$ with respect to the $\hat{x}$ axis. We find that the diffusion is isotropic only when the average displacement of fluid monomers is less than the stripe width. When $r_\theta \gtrsim a$, the mean square displacement curves exhibit a gradual crossover to a linear regime ($r_\theta^2 \sim t$) where the diffusion becomes anisotropic. Averaging over long time periods (up to $2.6 \times 10^7 \, \tau \approx 5.6 \times 10^{-5}$ s) was required to accumulate good statistics because of the relatively low probability that a fluid monomer would remain in the first layer for a long time, especially above the nonwetting regions where the fluid density layering is reduced and fluid monomers jump in and out of the first layer more frequently.

The diffusion coefficient was computed from the linear slope of the mean square displacement as a function of time ($r_\theta^2 = 4D_\theta t$) in the regime $t \gtrsim 145\tau$, which is shown in more detail in the lower inset of Fig. 8. The slight nonlinearity in MSD curves at large times is reflected in the error bars for the diffusion coefficient. Most interestingly, as shown in the upper inset of Fig. 8, there is an almost linear correlation between the in-plane diffusion coefficient and the effective slip length as a function of θ. It means that the longitudinal component of the slip velocity along the shear flow direction is proportional to the diffusion rate of fluid monomers along that direction at equilibrium. The results in Fig. 8 provide support for the
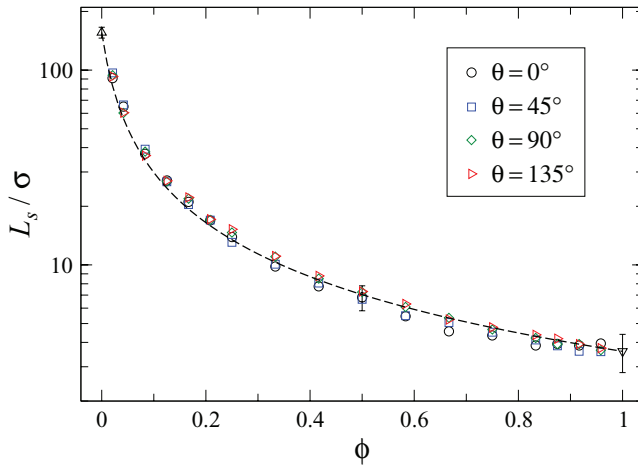
FIG. 9. The effective slip length L_s/σ versus the fraction of randomly distributed attractive atoms ($\delta = 1.0$) at the lower wall. The orientation of the upper wall velocity is specified in the inset. The black dashed curve is Eq. (8) with $b_w(\phi = 1) = 3.6\sigma$ and $b_n(\phi = 0) = 156\sigma$.

FIG. 10. The mean square displacement of fluid monomers in the first layer near the lower wall with $\phi = 0$, 0.08, 0.58, 0.75, 1.0 (from left to right) when $U = 0$. The dashed line with unit slope is plotted as a reference. The inset shows a typical trajectory of a fluid monomer for about 100τ near the wetting wall $\phi = 1.0$. The positions of the fcc lattice atoms in the xy plane are denoted by open circles.

microscopic justification of the tensorial formulation of the Navier slip boundary condition in the case of Newtonian fluids and molecular-scale surface textures. A similar correlation between D_θ and L_s also holds for smaller stripe widths ($a = 0.74\sigma$ and $a = 1.47\sigma$), although the difference in diffusion rates along $\theta = 0°$ and $90°$ directions becomes smaller when the stripe width decreases (not shown). For larger stripe widths ($a = 4.42\sigma$ and $a = 8.84\sigma$), an accurate resolution of the mean square displacement curves in the linear regime ($r_\theta > a$) would require a long averaging time because of the low probability that a fluid monomer will remain within the first layer for a long time interval.

D. Slip flows over surfaces with random textures

In general, the problem of slip flow over surfaces with mixed boundary conditions specified on randomly distributed regions is difficult to treat either analytically or numerically. An example of a statistical analysis of the effective slip boundary condition for liquid flow over a plane boundary with randomly distributed free-slip regions was presented in Ref. 54. It was found that the effective slip length is proportional to the typical size of free-slip regions and a factor that depends on the fractional area coverage.[54] In this section, we consider a simple shear flow over a smooth substrate with random distribution of wetting and nonwetting regions. The system setup is essentially the same as described in Sec. II, except that the parameter δ in Eq. (2) is randomly chosen to be either 0.1 or 1.0 for the lower wall atoms. Each of the two fcc lattice layers of the lower wall contains the same number of weakly ($\delta = 0.1$) or strongly ($\delta = 1.0$) attractive atoms. In what follows, a fraction of wall atoms with $\delta = 1.0$ is denoted by ϕ. Due to limited computational resources, only one realization of disorder was considered for each value of ϕ.

Figure 9 shows the effective slip length as a function of ϕ for four orientations of the upper wall velocity relative to the lower wall. As expected, L_s decreases with increasing the total area of wetting regions. Note that for each value of ϕ, the flow is almost isotropic; the slight discrepancy is most prob-
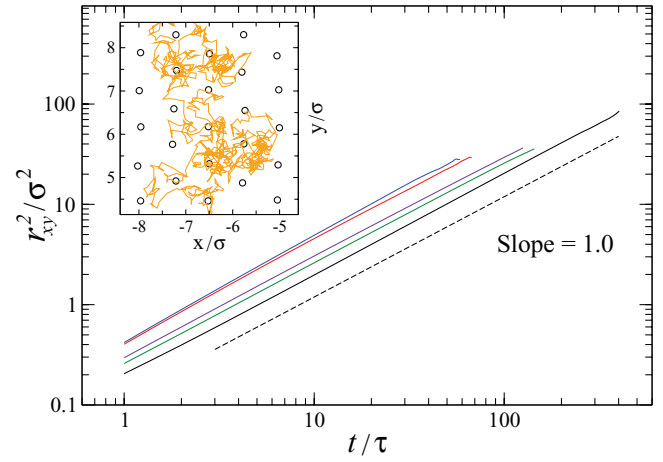
ably due to finite size effects. When $\phi = 0.5$, the averaged effective slip length $L_s \approx 7.0\sigma$ is between $b_\perp$ and $b_\parallel$ for any value of the stripe width reported in Figs. 5 and 7, which confirms earlier conclusions that parallel (perpendicular) stripes attain maximum (minimum) slippage. In the limiting cases $\phi \to 0$ or $\phi \to 1$, the fluid velocity fields near the lower wall are parallel to the xy plane, and the total friction coefficient (the ratio of fluid viscosity to slip length) can be estimated by simply adding contributions from wetting and nonwetting areas as follows:

$$\frac{\mu}{L_s(\phi)} = \frac{\mu\,\phi}{b_w} + \frac{\mu\,(1-\phi)}{b_n}, \qquad (7)$$

where b_w and b_n are, respectively, the slip lengths for wetting ($\phi = 1$) and nonwetting ($\phi = 0$) surfaces. This immediately gives the effective slip length as a function of ϕ

$$L_s(\phi) = \frac{b_w\,b_n}{\phi\,b_n + (1-\phi)\,b_w}. \qquad (8)$$

As shown in Fig. 9, the agreement between the MD data and Eq. (8) is quite good for all ϕ in the range [0, 1]. However, this correspondence might, in general, not hold at intermediate values of ϕ and larger system size in the $\hat{x}$ and $\hat{y}$ directions because of the spatial variation of velocity profiles induced by the heterogeneous surface. Interestingly, the formula for the effective friction coefficient, Eq. (7), also accurately describes hydrodynamic flows along alternating stripes with local slip lengths that are larger than the system size.[30,55] In addition, it was shown numerically that an interpolation formula like Eq. (7) predicts the effective slip length for composite interfaces which consist of periodically distributed solid and gas areas.[56]

Similar to the analysis of the interfacial diffusion presented in Sec. III C, we evaluate the in-plane diffusion coefficient in the absence of shear flow for fluid monomers in the first layer near the lower wall for the same realization of disorder as in Fig. 9. As an example, a typical trajectory projected onto the xy plane is shown in the inset of Fig. 10.
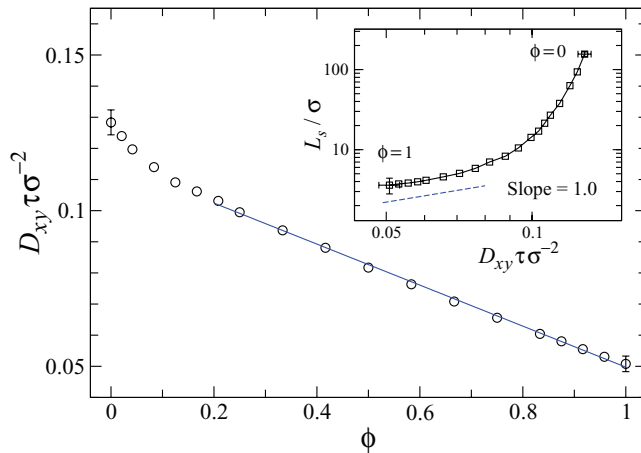
FIG. 11. The in-plane diffusion coefficient D_{xy} (in units σ^2/τ) as a function of ϕ. The straight blue line is the best fit to the data for $\phi > 0.2$. The inset shows a correlation between the effective slip length and the diffusion coefficient for $0 \leq \phi \leq 1$. The solid curve is a guide for the eye. The dashed line with unit slope is drawn for reference.

It can be seen that when $\phi = 1$, the diffusive motion of a fluid monomer in contact with lower wall atoms is strongly influenced by the periodic surface potential; most of the time the monomer resides near the local minima of the surface potential. In this case, the surface-induced structure in the first fluid layer is quantified by a distinct peak in the structure factor at the main reciprocal lattice vector $S(8.53\sigma^{-1}, 0) \approx 1.7$, which is comparable to the height of a circular ridge $S(2\pi/\sigma) \approx 2.9$ characteristic of the short range order. As the fraction of wetting regions decreases, the amplitude of density oscillations near the lower wall is reduced [see Fig. 3(a)], trajectories of fluid monomers become less affected by the corrugation of the random surface potential, and the time interval between jumps in and out of the first fluid layer decreases. When $\phi \lesssim 0.08$, the in-plane structure factor, estimated in the first fluid layer at equilibrium, does not contain any peaks at the reciprocal lattice vectors.

The mean square displacement curves as a function of time are displayed in Fig. 10 for selected values of ϕ. It is apparent that the diffusion becomes faster as the total area of nonwetting regions increases. The in-plane diffusion coefficient was estimated from the Einstein relation $r_{xy}^2 = 4D_{xy}t$ when $t \gtrsim 6\tau$. As shown in Fig. 11, the diffusion coefficient gradually varies between two values obtained for homogeneous surfaces with $\phi = 0$ and $\phi = 1$. Furthermore, a correlation between the effective slip length (averaged over four orientations of the mean flow) and the in-plane diffusion coefficient is presented in the inset of Fig. 11. These data indicate a nearly linear dependence between L_s and D_{xy} when the fraction of wetting regions is large, and, as discussed earlier, there is a strong coupling between the diffusion of fluid monomers in the first layer and the periodic surface potential. In the opposite limit of small ϕ, the net adsorption energy is reduced and the in-plane diffusion of fluid monomers is mostly dominated by the interaction with its fluid neighbors. In this regime, the effective slip length increases rapidly as the fraction of wetting regions decreases.

IV. CONCLUSIONS

In this study, molecular dynamics simulations were performed in order to investigate the effective slippage and molecular diffusion at surfaces patterned with periodic or random textures. In our setup, the typical size of surface patterns is smaller than the channel dimensions, and the local boundary conditions at homogeneous wetting or nonwetting surfaces are described by finite slip lengths. Particular attention was paid to the implementation of a thermostatting procedure that does not bias flow profiles and diffusion of fluid monomers.

For flows over surfaces patterned with stripes of different wettability, the heterogeneous surfaces induce wavy perturbations in velocity profiles and the slip velocity acquires a transverse component. In this case, the effective slip length depends on the shear flow direction with respect to the stripe orientation. We found that the angular dependence of the effective slip length computed by molecular dynamics simulations agrees well with the analytical solution of the Stokes equation provided that the stripe width is larger than several molecular diameters. At the same time, however, the ratio of the transverse and longitudinal components of the slip velocity agrees only qualitatively with hydrodynamic predictions. Furthermore, the interfacial diffusion coefficient of fluid molecules correlates well with the effective slip length as a function of the shear flow direction. The numerical analysis was performed only for fluid monomers that remain in contact with the wall atoms during the diffusion time interval. These findings lend support for the microscopic justification of the tensor formulation of the effective slip boundary conditions for noninertial flows of Newtonian fluids over smooth surfaces with nanoscale anisotropic textures.

In case of random surface textures, the simulation results and simple physical arguments show that the effective slip length is determined by the total area of wetting regions. When the fraction of wetting regions is large, the diffusive motion of fluid monomers is strongly influenced by the periodic surface potential, and the effective slip length is nearly proportional to the in-plane diffusion coefficient at equilibrium. In the opposite limit of small wetting areas, the diffusion of fluid monomers is less affected by the corrugation of the surface potential, and the effective slip length depends sensitively on the number of strongly attractive wall atoms.

[1]A. D. Stroock, S. K. Dertinger, G. M. Whitesides, and A. Ajdari, Anal. Chem. **74**, 5306 (2002).
[2]T. M. Squires and S. R. Quake, Rev. Mod. Phys. **77**, 977 (2005).
[3]L. Bocquet and E. Charlaix, Chem. Soc. Rev. **39**, 1073 (2010).
[4]N. V. Churaev, V. D. Sobolev, and A. N. Somov, J. Colloid Interface Sci. **97**, 574 (1984).

[5]C. Cottin-Bizonne, B. Cross, A. Steinberger, and E. Charlaix, Phys. Rev. Lett. **94**, 056102 (2005).

[6]O. I. Vinogradova and G. E. Yakubov, Phys. Rev. E **73**, 045302 (2006).

[7]H. Li and M. Yoda, J. Fluid Mech. **662**, 269 (2010).

[8]L. Zhu, P. Attard, and C. Neto, Langmuir **27**, 6712 (2011).

[9]J. Ou, B. Perot, and J. P. Rothstein, Phys. Fluids **16**, 4635 (2004).

[10]P. Joseph, C. Cottin-Bizonne, J.-M. Benoit, C. Ybert, C. Journet, P. Tabeling, and L. Bocquet, Phys. Rev. Lett. **97**, 156104 (2006).

[11]R. Truesdell, A. Mammoli, P. Vorobieff, F. van Swol, and C. J. Brinker, Phys. Rev. Lett. **97**, 044504 (2006).

[12]C. Lee and C. J. Kim, Langmuir **25**, 12812 (2009).

[13]U. Heinbuch and J. Fischer, Phys. Rev. A **40**, 1144 (1989).

[14]J. Koplik, J. R. Banavar, and J. F. Willemsen, Phys. Fluids A **1**, 781 (1989).

[15]P. A. Thompson and M. O. Robbins, Phys. Rev. A **41**, 6830 (1990).

[16]P. A. Thompson and S. M. Troian, Nature (London) **389**, 360 (1997).

[17]J.-L. Barrat and L. Bocquet, Phys. Rev. Lett. **82**, 4671 (1999).

[18]J.-L. Barrat and L. Bocquet, Faraday Discuss. **112**, 119 (1999).

[19]K. P. Travis and K. E. Gubbins, J. Chem. Phys. **112**, 1984 (2000).

[20]V. P. Sokhan, D. Nicholson, and N. Quirke, J. Chem. Phys. **115**, 3878 (2001).

[21]T. M. Galea and P. Attard, Langmuir **20**, 3477 (2004).

[22]N. V. Priezjev, Phys. Rev. E **75**, 051605 (2007).

[23]N. V. Priezjev, J. Chem. Phys. **127**, 144708 (2007).

[24]C. Y. Soong, T. H. Yen, and P. Y. Tzeng, Phys. Rev. E **76**, 036303 (2007).

[25]C. Liu and Z. Li, Phys. Rev. E **80**, 036302 (2009).

[26]N. Asproulis and D. Drikakis, Phys. Rev. E **81**, 061503 (2010).

[27]A. A. Pahlavan and J. B. Freund, Phys. Rev. E **83**, 021602 (2011).

[28]S. K. Kannam, B. D. Todd, J. S. Hansen, and P. J. Daivis, J. Chem. Phys. **135**, 144701 (2011).

[29]N. V. Priezjev, Phys. Rev. E **82**, 051603 (2010).

[30]C. Cottin-Bizonne, C. Barentin, E. Charlaix, L. Bocquet, and J. L. Barrat, Eur. Phys. J. E **15**, 427 (2004).

[31]N. V. Priezjev, A. A. Darhuber, and S. M. Troian, Phys. Rev. E **71**, 041608 (2005).

[32]T. Z. Qian, X. P. Wang, and P. Sheng, Phys. Rev. E **72**, 022501 (2005).

[33]S. C. Hendy, M. Jasperse, and J. Burnell, Phys. Rev. E **72**, 016303 (2005).

[34]A. Niavarani and N. V. Priezjev, Phys. Rev. E **81**, 011606 (2010).

[35]N. V. Priezjev and S. M. Troian, J. Fluid Mech. **554**, 25 (2006).

[36]A. Niavarani and N. V. Priezjev, J. Chem. Phys. **129**, 144902 (2008).

[37]C. Jeon, H. Jeong, and Y. Jung, Phys. Rev. E **83**, 056324 (2011).

[38]C. Y. Wang, Phys. Fluids **15**, 1114 (2003).

[39]C. J. Teo and B. C. Khoo, Microfluid. Nanofluid. **7**, 353 (2009).

[40]A. V. Belyaev and O. I. Vinogradova, J. Fluid Mech. **652**, 489 (2010).

[41]M. Z. Bazant and O. I. Vinogradova, J. Fluid Mech. **613**, 125 (2008).

[42]K. Kamrin, M. Z. Bazant, and H. A. Stone, J. Fluid Mech. **658**, 409 (2010).

[43]O. I. Vinogradova and A. V. Belyaev, J. Phys.: Condens. Matter **23**, 184104 (2011).

[44]K. Kamrin and H. A. Stone, Phys. Fluids **23**, 031701 (2011).

[45]F. Feuillebois, M. Z. Bazant, and O. I. Vinogradova, Phys. Rev. Lett. **102**, 026001 (2009).

[46]F. Feuillebois, M. Z. Bazant, and O. I. Vinogradova, Phys. Rev. E **82**, 055301(R) (2010).

[47]N. K. Ahmed and M. Hecht, J. Stat. Mech.: Theory Exp. P09017 (2009).

[48]M. P. Allen and D. J. Tildesley, *Computer Simulation of Liquids* (Clarendon, Oxford, 1987).

[49]R. Khare, J. de Pablo, and A. Yethiraj, J. Chem. Phys. **107**, 2589 (1997).

[50]D. Toton, C. D. Lorenz, N. Rompotis, N. Martsinovich, and L. Kantorovich, J. Phys.: Condens. Matter **22**, 074205 (2010).

[51]W. D. Kaplan and Y. Kauffmann, Annu. Rev. Mater. Res. **36**, 1 (2006).

[52]E. Lauga and H. A. Stone, J. Fluid Mech. **489**, 55 (2003).

[53]H. Bock, K. E. Gubbins, and M. Schoen, J. Phys. Chem. C **111**, 15493 (2007).

[54]M. Sbragaglia and A. Prosperetti, J. Fluid Mech. **578**, 435 (2007).

[55]S. C. Hendy and N. J. Lund, Phys. Rev. E **76**, 066313 (2007).

[56]C. Ybert, C. Barentin, C. Cottin-Bizonne, P. Joseph, and L. Bocquet, Phys. Fluids **19**, 123601 (2007).